Energy Conversion and Management 323 (2025) 119191

Contents lists available at ScienceDirect

Energy Conversion and Management

journal homepage: www.elsevier.com/locate/enconman

Comparative analysis of powertrain architectures for fuel cell light commercial vehicles in terms of performance and durability

R. Novella, M. Lopez-Juarez *, D. González-Domínguez, I. Nidaguila

CMT-Motores Térmicos, Universitat Politècnica de València, Camino de vera s/n, 46022 Valencia, Spain

ARTICLE INFO

Keywords:
Hydrogen
Proton exchange membrane fuel cell
Light commercial vehicle
Performance
Durability
Powertrain sizing

ABSTRACT

At the present time, the critical climate situation has raised awareness about the importance of developing carbon-free technologies. In this context, fuel cell systems (FCS) have become one of the key technologies in the pathway to decarbonization. Given that road transport is a major contributor to greenhouse gas (GHG) emissions, this paper focuses on a specific segment of this sector: light commercial vehicles (LCVs). The current market situation shows that LCV manufacturers have not yet decided what is the appropriate powertrain architecture for this kind of vehicle. Thus, the current paper studies a wide range of possible FCS-based propulsive system designs, changing the size of the FCS, electric battery and H_2 tank. These propulsive system architectures are analyzed concerning the performance of the vehicle, in terms of consumption and range, and the durability of its FCS. The evaluation of these different designs will be highly valuable for the LCV industry and manufacturers, as it allows to understand the optimal powertrain solution. The study demonstrates that a significant increase in range can be achieved with only a minor penalty in hydrogen consumption. Additionally, the research indicates that it is feasible to employ one of the most durable FCS designs while meeting LCV mission requirements with minimal consumption penalty. In conclusion, this paper provides valuable data to the ongoing research in this field, offering a detailed analysis of the impact of H_2 consumption, autonomy, and durability of the FCS across various vehicle architectures under typical LCV driving conditions.

1. Introduction

At present times, the world is facing an environmental crisis caused by the increasing amount of greenhouse gases (GHG) and the rapid depletion of natural resources. This critical situation has raised awareness about the need to develop clean energies to ease the decarbonization of the industry and global institutions are working together to elaborate different strategies that aim to solve this issue [1]. In this context, the transportation sector stands out as a significant contributor to global GHG emissions, accounting for approximately one quarter of the total emissions [2].

One of the energy carriers that has acquired importance during the past few years is hydrogen, which can be used for very different applications and could have a low carbon footprint [3] depending on its production pathway, as studied in [4]. The energy production process using H_2 can be done by using FCS [5] or by H_2 combustion in an ICE [6]. At the present time, both FCS and H_2 ICE have presented themselves as a good solution in the decarbonization of road transportation. In this context, the use of FCS usually comes together with an electric battery, integrated in a hybrid vehicle, but it can also be used as a range-extender or as the main power source coupled with a small battery for brake recovery.

Focusing on the road transportation sector, manufacturers seem to have reached a consensus about the use of FCS in heavy-duty (HD) vehicles and some prototypes are starting to reach the market as the Hyundai XCIENT Fuel Cell. There currently exists a modular trend in which different FCS are integrated into the powertrain of the truck and are its main power source, which works together with a smaller electric battery [7]. The mentioned architecture tendency has led to the use of a set of small or medium power FCS. In previous works, the current research group has analyzed one of this HD-designed FCS [8]. In the HD sector, the need to maximize range as well as refuel time is decreased, is crucial and it is the main reason behind the use of FCS for this application. Despite the great potential of these technologies, its inclusion into the HD market sector is still a matter of research that some authors are currently studying, as Yan et al. in [9]. Thus, as with other FCS-based technologies, its related emissions are an essential issue that also needs to be considered so that its use is as clean as possible. Thus, several researchers are also looking into this topic, as in [10,11].

* Corresponding author.
E-mail address: marlojua@mot.upv.es (M. Lopez-Juarez).
URL: https://www.cmt.upv.es (M. Lopez-Juarez).

https://doi.org/10.1016/j.enconman.2024.119191
Received 25 July 2024; Received in revised form 13 October 2024; Accepted 22 October 2024
Available online 4 November 2024

In the HDV sector the propulsive system for FCVs seems to follow the same trend, modular FCS as the main power source couple with a small electric battery. Thus, in this field, authors are now focusing on the control strategy between the different FCS and the battery [12], rather than studying the sizes of each component of the powertrain. Researches are following different approaches regarding the energy management strategies (EMS). Some authors as Chen et al. have tested the use of dynamic programming (DP) as in [13]. Other researchers are starting to study predictive strategies that would allow to obtain results which would be more similar to a real driving situation, as in [14,15]. In [16], Agyekum et al. analyze the research tendencies regarding FC technologies along the past decades. In this piece of work, the authors agree that the current trends usually focus on the optimization of the control of the FCS vehicle by the improvement of the EMS [17] using machine learning. The existing optimization strategies of FCVs also cover architecture-related subjects, mainly focused on the thermal management of the powertrain [18]. Additionally, H_2 clean production [19], distribution and refueling stations [20] represent a topic of interest regarding these vehicles.

The HD field has been deeply studied during the last few years, besides there are other vehicle sectors in which FCS would be appropriate and have not been analyzed in detail. Focusing on the road transportation sector, the use of FC technologies in passenger cars has also been widely studied during the past years [21]. However, the study of FCS in light commercial vehicles (LCVs) is a quite unexplored field. The little existing bibliography seems to follow the common trends regarding FCVs. In [22], Skarlis et al. analyze different refueling strategies. In [23], Apostolou et al. compare the refueling of the LCV H_2 tank by using different storage systems. Thus, the H_2 well-to-tank pathway has been the main topic of interest regarding these vehicles.

LCVs or vans are designed for intensive use in the commercial sector, which makes clear that the use of FCS would be extremely benefitial. However, their power demand is significantly lower compared to that of trucks. Thus, it is still not clear which kind of powertrain would be more appropriate for them. The currently existing prototypes are quite different between each other. Some companies propose a range-extender configuration as the Renault Kangoo Z.E. Hydrogen, which includes a 5 kW FCS to increase autonomy. This company has also developed the Renault Master Z.E. Hydrogen [24], with a range-extender configuration that allows a higher range by including a 33 kWh electric battery coupled with a 30 kW FCS and a 4.2 kg H_2 tank. Nevertheless, other vehicle manufacurers as Opel (Opel Vivaro Hydrogen van) have chosen a mid-power architecture composed of a bigger FCS (45 kW) and a smaller battery (10.5 kWh) with a 4.4 kg tank [25]. Even some companies are trying different approaches by retrofitting an existing vehicle (Toyota HiAce [26]) or using solid oxide FC (existing prototype by Nissan [27]). However, in this context FCS have proven to be one of the most popular options among vehicle manufacturers. Nevertheless, there exist different kind of FC which can be classified depending on the electrolyte they use. Alkaline fuel cells (AFCs) use potasium hydroxide (KOH), they were the first FC technology to be developed and gave good results in the production of energy for the space programme. However, AFCs can be easily poisoned by CO_2 concentrations, which represents an important problem when using ambient air. Phosporic Acid Fuel Cells (PAFCs) were one of the first technologies to be commercialized, but their low power production implies that they need to be large, heavy and expensive to be efficient enough in its use [28]. Additionally, other kind of FC as Molten Carbonate Fuel Cells (MCFCs) and Solid Oxide Fuel Cells (SOFCs) work under high temperatures. These kind of high temperature cells have shown promising results, but its low startup process makes them unappropriate for road transportation application. In this context, Polymer Electrolyte Membrane Fuel Cells (PEMFCs) present themselves as a good choice for road vehicle applications. As opposed to other fuel cells, PEMFCS have low weight and volume and provide high power density using a noble-metal catalyst (such as Pt) [29]. Thus, the authors have chosen to model the FCS as a PEMFCs. The use of PEMFCs for road applications is very popular at the present times and there exist a high research interest in the study of the used materials in this kind of FCs [30].

After an initial review of the market sector, it is important to study in detail the existing research literature about the use of FCS in the LCV industry. There currently exists little research papers about this kind of vehicles. Concerning road transportation, most studies focus on the analysis of HDVs [31] rather than LCVs. The existing papers related to this market sector focus on economic [32] or emission [33] studies, rather than performing a detailed study of the performance of the vehicle.

Furthermore, the extisting pieces of research that study the architecture of the LCV are mainly focused on the H_2 storage [34] or the refueling system [35]. Additionally, the limited number of papers that examine various powertrain architectures [36] or focus on vehicle performance [37] utilize FCS models with a low level of detail. This is because such studies aim to provide a broad overview or focus on other aspects, such as energy management strategies, as explained for HDVs, rather than conducting a detailed sizing study of the powertrain.

Therefore, the understanding of the influence of each powertrain component in a LDFCV (Light-duty Fuel Cell Vehicle) would be significant for the existing bibliography. The analysis of the powertrain would require the study of the factors that define the mission of the vehicle. As in any vehicle, the fuel consumption is a key matter to define its performance. The minimization of H_2 consumption has been studied by different researchers for other vehicle sectors and by applying different methodologies, as in Hu et al. in [38]. As previously stated, LCVs are used in an intensive way, thus, its mission is defined by the range the are able to cover with a fixed amount of fuel. Additionally, a key issue in the use of FCS is its lifetime. As with any other technology that is still in development, there are still problems to be resolved and the degradation of the cells is an essential matter that is being looked into. The research community has approached this issue in different ways by modeling degradation as in [39] and measuring experimental data as in [40]. The evaluation of the 3 stated parameters: H_2 consumption, range of the vehicle and durability of the FCS would allow to understand the vehicle suitability for a specific mission. Nevertheless, there exist no available studies that analyze these parameters for a LDFCV.

1.1. Knowledge gaps

Considering the available data and studies in the literature seen in Section 1, the following knowledge gaps have been identified in this research line.

1. There is a significant gap in the detailed data regarding the actual fuel consumption rates of FCS when integrated into the propulsion systems of LCVs. This information is critical for optimizing fuel efficiency and overall vehicle performance.
2. Detailed knowledge about the range of hybrid LCVs that are composed of both FCS and electric batteries is sparse. Knowing the distance each component can provide independently, as well as their combined range, is crucial for designing efficient and practical vehicles
3. Comprehensive data on the durability and lifespan of complete FCS is limited. Furthermore, there is even less information available regarding the durability of these systems when they are part of a hybrid powertrain (combining FCS and an electric battery) tailored for the specific operational requirements of LCVs.
4. There is a lack of clarity and consensus on which powertrain configuration offers the optimal performance for the specific mission of an LCV.

Based on the preceding analysis, it is evident that there exists a notable scarcity of research concerning the integration of FCS into LCVs, indicating significant knowledge gaps in this area. In Section 1, the authors have provided a summary of the existing research regarding the use of FCs in LCVs, which shows the literature gap about the powertrain architecture. Addressing this limitation would offer valuable insights for researchers and LCV manufacturers, thereby playing a crucial role in the decarbonization of this sector.

1.2. Contribution and objectives

This paper aims to understand the influence of different designs for an FCS powertrain in an LCV. The specific contributions to achieve such an objective are:

- Analysis of the H_2 consumption by each of the different proposed architectures. The amount of used H_2 allows to select an efficient powertrain design, considering the efficiency in fuel utilization. Furthermore, this value is essential in future cost or emission studies.
- Evaluate the range of FC-powered LCVs. Since the proposed vehicle architectures are FC hybrid vehicles, the autonomy provided by each energy source will be computed to determine the value provided by the final vehicle architecture. This analysis aims to assess whether the chosen vehicle architecture meets the mission requirements rather than achieving the maximum possible range.
- Study the durability of the FCS for each of the different proposed designs in an LCV. This is possible by the use of a degradation model integrated into the simulation platform used to recreate the desired driving conditions. As with H_2 consumption, this is a critical parameter for future FCV studies.
- Overall comparison of the different propulsive system architectures. The final goal behind this analysis is to set a basis for what would be the most appropriate design for an LCV considering its usual mission.

The accomplishment of the previously stated tasks would lead to the achievement of the final goal of this study and filling the current knowledge gaps in the field (Section 1.1). The accomplishment of the set objectives already represents a novelty in comparison to the existing literature. However, the methodology employed (Section 2) is based on models developed by the authors, which form a virtual LCV vehicle that is representative of a real FCS vehicle and stands out from the models found in the literature.

In summary, the present paper will provide a representative set of data about different LCV architectures, which will have both a high research and industrial value. Furthermore, it will give an insight about which could be the best powertrain architecture for an LCV mission.

2. Methodology

The present study evaluates the effect of varying the FC stack power, H_2 tank and battery size on performance and durability while maintaining range and load capacity at acceptable levels for an LCV. The platform used to achieve this objective comes from the combination of different models that have already been developed and tested during previous studies. The final model integrates all the necessary components to simulate the behavior of a real FCV. On the one hand, a light-duty vehicle is modeled in GT-Suite v2020 and is coupled with a Simulink empirically checked FCS model based on a real FC powertrain (Section 2.1.1). On the other hand, to simulate in realistic conditions the chosen driving cycles, the simulation platform also integrates EMS algorithms and a semi-empirical degradation model [41]. The present section explains each part of the used simulation tool. The methodology followed throughout the paper is summarized in Fig. 1.

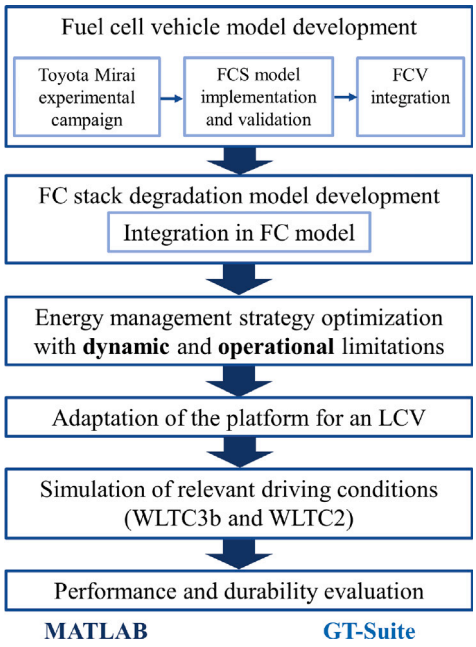

Fig. 1. H_2 consumed in the WLTC3b driving conditions with a 4 kg H_2 tank.

For a higher level of detail, the specific studies that were used to generate each model are referred in this piece of work. The integration between the components and the FCS is explained in further detail because it represents an important novelty in the simulation architecture.

2.1. Fuel cell vehicle

The main parts in the modeling of the vehicle are the powertrain, the vehicle architecture, and the driver. The present study focuses on the change of the propulsive system. However, the weight of this system should not be neglected when considering the vehicle architecture. Thus, the simulation platform relates all the involved elements of the vehicle to resemble a real LCV.

The electric battery and vehicle architecture are implemented in GT-Suite. This software represents a powerful tool that is widely used nowadays in the automotive industry. It solves the continuity, momentum, energy, and species equation numerically and applies common physically-based correlations to model 0D-1D thermal fluid-dynamics. One of its advantages is its linkability to other softwares. This property allows the creation of the already mentioned simulation platform, which integrates different MATLAB R2022a models.

In addition, the driver is also integrated into the GT-Suite model. This is an easy way to include the desired driving conditions because this software includes standardized driving cycles for a wide variety of road transportation sectors.

Finally, the FCS model used requires a deeper explanation. The developed simulation tool is presented in Section 2.1.1, but for a detailed review of each part of the model can be found in [42].

2.1.1. Fuel cell model

The FCS model used in the performed analyses consists of a MATLAB-Simulink tool [42] that has been calibrated with a public experimental dataset obtained from Argonne National Laboratory (ANL). The present model has been calibrated in dynamic conditions for standarized driving profiles (WLTC3b and US06), which allows to have highly precise results in the simulation of a FCS integrated in a vehicle. This model will be explained in further detail in the present section. However, it is important to remark that for the present paper

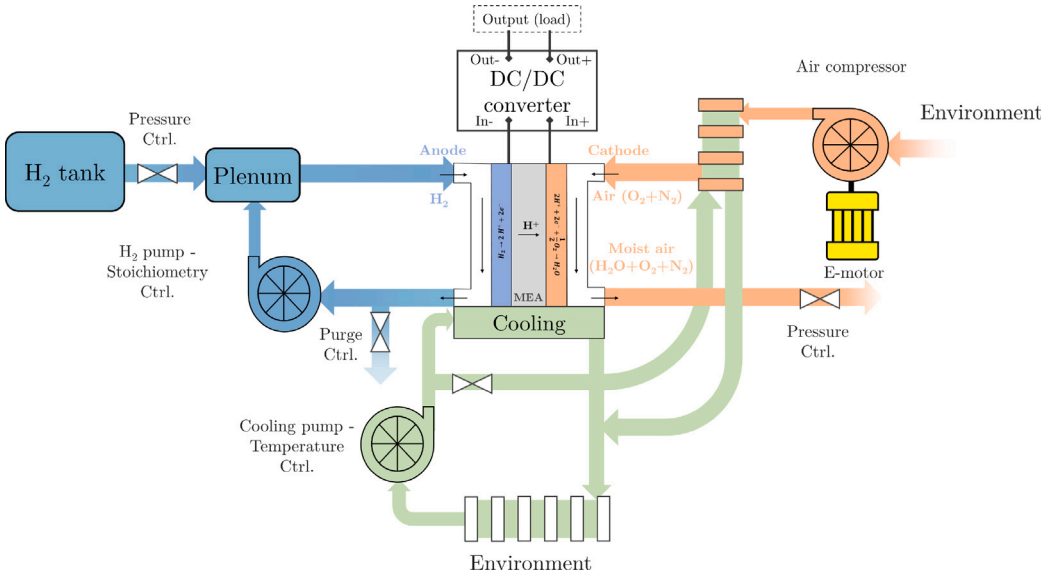

Fig. 2. Fuel cell system model outline: main components in the anode, cathode, and cooling systems [42].

the FCS was scaled to be adaptative for different number of cells in the stack. Furthermore, additional elements were also added to the air path to ensure its correct operation.

The used dataset has enabled a precise calibration of an FCS realistic model, but these results have not allowed a full acknowledgment of all the parameters that should be taken into account in an FCS. Some of the unknown variables or mechanisms that take place in the system have been calculated or estimated. The present article focuses on making a sum up of the main characteristics of the FCS for a better understanding of the performed study.

The FCS is based on the one included in the Toyota Mirai. Thus, it is divided into 4 main parts which are designed to match the performance of this specific system: anode circuit, cathode circuit, cooling system, and FC stack. The whole system is represented in detail in Fig. 2.

The FC stack is mainly divided in two parts: the bipolar plates and the MEA or membrane electrode assembly. The present model uses the conditions at the anode and cathode bipolar plates to compute a polarization curve by using the quasi-steady-state electrochemical model given by the MEA. The model used to calculate the voltage in the polarization curve considers both the voltage from Nerst equation (electrochemical reaction in the MEA) and the voltage losses in the FC stack (Eq. (1)).

$$V_{FC} = V_{Nerst} - V_{OC} - V_{act} - V_{ohm} - V_{conc} \quad (1)$$

The anode circuit is the part of the system in which the H_2 flow occurs. It is composed of different elements that go from the supply tank until the H_2 reaches the stack. This circuit has an active recirculation system, it uses a purge valve to remove the accumulated gas in the anode, which gets contaminated by species coming from the cathode from time to time, but it also uses a plenum to keep the H_2 flowing and avoid pressure oscillations.

The cathode or air circuit is more complex. The air mass flow goes into the cathode from the environment and passes through a compressor which regulates the amount of air going into the system (cathode stoichiometry), but it also adjusts its pressure to the appropriate conditions in the bipolar plates. After that, the air circuit passes through a heat exchanger to ensure the temperature in the stack is inside the operating limits, usually between 50 and 80 °C. The air that flows out of the cathode is controlled by the opening of a pressure valve. This system does not include a humidifier, as other FCS, because this specific model is based on the functioning of the BoP included in the Toyota Mirai FCS.

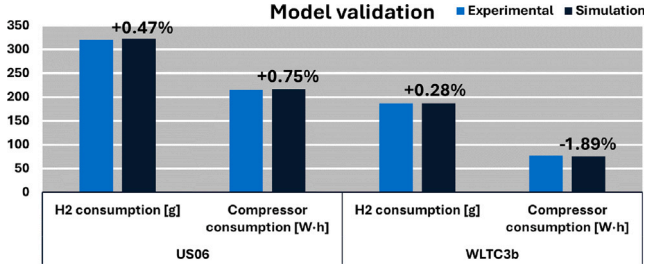

Fig. 3. Error between the experimental and simulation values in the validation of the FCS model [42].

Finally, the cooling system is used to control the temperature of the system. This includes a pump to make the coolant flow along the pipes and two heat exchangers. One heat exchanger is in contact with the environment to control the temperature of the coolant and the other controls the temperature in the cathode. This system is also directly in contact with the stack because its temperature is critical in the functioning of the system.

After the stack and the BoP have been designed and integrated into a model, the simulation tool has to be calibrated. The first step in the calibration of an FCS is to get an approximation of the polarization curve. Some steady-state tests under different conditions allow to calibrate the performance of the main parts of the system: anode, cathode, and cooling circuits. After that, the use of dynamic tests allows the improvement of the results in what is called, recalibration process.

Finally, the simulation tool is validated by comparing the model with experimental data from driving conditions characteristics of the real operation of this kind of vehicle, WLTC3b and US06 driving cycles. The results from these tests show an error between the simulation and the experimental data which is lower than a 2%. Fig. 3 shows the total errors achieved in the tested driving conditions. This small error in different driving conditions allows the use of this model to simulate the performance of an FCS in a vehicle.

2.1.2. Vehicle architecture

The vehicle used as a reference to model the studied LCV is the Renault Master Z.E. Hydrogen. This vehicle has been chosen because it is one of the few currently commercialized hydrogen vans. Therefore, it can be said that it is a good representation of the existing market trend

Table 1
Reference data for the light-duty FCV based on the Renault Master Z.E. Hydrogen [24,43].

	Dimensions
Wheel base	4.332 m
Length	6.225 m
Width	2.470 m
Height	2.850 m
	Weight
Min. kerb weight	2854 kg
Max. weight	3940 kg
Payload	1086 kg
	H_2 tank
Service pressure	700 bar
Max. tank pressure	850 bar
Capacity	6.4 kg
	Battery
Technology	Z.E. 33 Li-ion
Capacity	1 pack of 33 kWh
	Electric motor
Technology	R75
Capacity	57 kW (76 HP)

for hydrogen vehicles. Renault has also commercialized the Kangoo Z.E. Hydrogen, but for the purposes of this study, in which the goal is to maximize load capacity as well as range, the vehicle with a higher autonomy (Master Z.E) is chosen.

The Renault Master Z.E. Hydrogen is composed of an FC stack of 30 kW, an electrical battery of 33 kWh, its balance of plant (BoP), and vehicle architecture. It can be considered a range-extender way to use FC due to the maximum power of its FCS. However, the architecture of the vehicle will be used with different FC-battery arrangements. The detailed data used to model the architecture can be found in Table 1.

The mentioned architecture is used to model the main aspects of the vehicle. However, the powertrain design is modified to perform the desired study. Currently, there exist different market trends in the LCV sector which explore a wide variety of FC-battery arrangements, as explained in Section 1. This study aims to compare a wide set of distributions and analyze which would be the optimum type for an LCV. The proposed designs can be found in Fig. 4. The different sizes of the FCS, battery and H_2 conform a study matrix of 72 different vehicle architectures. This figure shows in red dots the different combinations of FCS and electric battery that will be tested. These combinations are simulated both for a 4 and 6 kg H_2 tank, as presented in the image. During previous simulation activities, smaller FCS (20 kW) were tested, but these architectures did not fulfill the charge-sustaining mode for the present vehicle and driving conditions. Thus, these smaller FCS configurations were discarded. Additionally, the maximum FCS power of 114 kW is considered enough to provide an appropriate vehicle range and an optimal efficiency. Increasing further the size of the FCS would lead to a weight increase without a clear benefit in FCS efficiency, which would be negative for the typical cargo mission of LCVs. These considerations allowed to establish the upper and lower limits in the powertrain architectures.

The FCS used is the model that has already been explained. However, the size of the FCS is also included in the GT-Suite model to consider its weight on the vehicle architecture. In addition, the battery is modeled in GT-Suite as a Li-ion battery pack. This element of the propulsive system is composed of a variable amount of cells depending on its size, but always with an efficiency of an 80%. The mentioned cells have a nominal voltage of 3.6 V and a capacity of 3.35 A h. Furthermore, depending on the propulsive system, the e-motor of the vehicle has a maximum power of either 60 or 120 kW. In each case, the gear ratio is optimized for the vehicle and specific driving conditions.

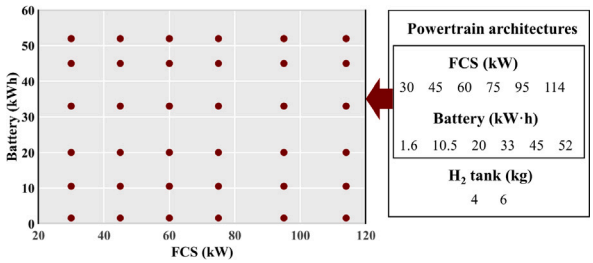

Fig. 4. Possible powertrain architectures to include in the LCV.

2.2. Energy management strategy

The EMS is the main algorithm that controls the power distribution in the simulated vehicle. The studied powertrain has two power sources in which the power is split: FCS and electric battery. The designed management strategy uses the Pontryagin Minimum Principle (PMP) to optimize the distribution in terms of a specific cost function [44], H_2 consumed by the FCS. This strategy allows to compare each of the different vehicle architectures in fair conditions because each of them is studied under its optimal performance by minimizing H_2 consumption [45].

The power demand made by the system can be shown in Eq. (2). The required value can come either from the FCS (P_{FCS}) or the battery (P_{bat}), but considering that the SOC of the second is charge sustained and should be 0.25. The control parameter u that should be minimum to control the H_2 consumption is the current density ($P_{FCS}(u)$).

$$P_{dem} = P_{bat} + P_{FCS} \tag{2}$$

Thus, the variable to be minimized is J (Eq. (3)), which represents the sum of the power consumed coming from H_2 during the whole time period.

$$J = \int_{t_0}^{t_f} P_f(u(t), t)\, \mathrm{d}t \tag{3}$$

In addition, the condition in Eq. (4) also needs to be met due to the charge sustained condition of the simulation. In this equation, P_b stands for the power consumed by the battery and E_b for its energy content.

$$\int_{t_0}^{t_f} P_b(u(t), E_b(t), t)\, \mathrm{d}t = 0 \tag{4}$$

According to PMP, a global optimization problem can be solved by local optimization. Thus, minimizing consumption for each time-step, would mean the obtention of the minimal consumption. The function to be minimized, is the Hamiltonian (Eq. (5)). In this expression, both P_f and $\dot{E}_b$ have the same units, so λ is dimensionless.

$$H = P_f - \lambda \cdot \dot{E}_b = P_f(u(t), t) + \lambda \cdot P_b(u(t), E_b(t), t) \tag{5}$$

In addition, a control parameter L is added to the equation to apply some dynamic restrictions to the operation. This restriction is shown in Eq. (6).

$$L = \begin{cases} 0 & |\mathrm{d}u/\mathrm{d}t|\,(t+\mathrm{d}t) \le |\mathrm{d}i/\mathrm{d}t|_{max} \\ \infty & |\mathrm{d}u/\mathrm{d}t|\,(t+\mathrm{d}t) > |\mathrm{d}i/\mathrm{d}t|_{max} \end{cases} \tag{6}$$

Considering all these conditions, a value of λ is established. This value allows to obtain the u that provides the minimum consumption for each time step and meets the SOC. Afterward, the process is repeated to optimize λ and obtain the optimal power distribution in Eq. (7).

$$H = P_f - \lambda \cdot \dot{E}_b + L \tag{7}$$

Table 2
Reference degradation rates (1st layer) to be scaled.

Condition	δ [fraction V loss]
Low power [/h] $\left(\frac{d\delta}{dt}\Big\|_{lp,ref}\right)$	$1.26 \cdot 10^{-5}$
Load change [/cycle] $\left(\frac{d\delta}{dn_{lc}}\Big\|_{ref}\right)$	$4.94 \cdot 10^{-7}$
High power [/h] $\left(\frac{d\delta}{dt}\Big\|_{hp,ref}\right)$	$1.03 \cdot 10^{-5}$
Start-stop [/cycle] $\left(\frac{d\delta}{dn_{ss}}\Big\|_{ref}\right)$	$1.95 \cdot 10^{-5}$

2.3. Degradation model

The overall performance of an FC vehicle is significantly linked to the degradation of its FCS. Thus, it is important to study how the specific driving conditions of an LCV would influence the degradation process of the simulated FC stack. For this purpose, a degradation model is integrated into the developed simulation tool. For a deeper explanation of the modeling framework, the research paper in which the used model is explained in detail can be found in [41]. The designed model computes in real time the voltage drop produced by the degradation of the stack, which is influenced by the operating conditions and the dynamics. To do this, the platform feeds it with the current density chosen by the EMS and the conditions of the system. In this way, the electrochemical mechanisms that are triggered both by the load of the system and the stack conditions can be considered.

The present degradation model is semi-empirical and it uses the experimental data (Table 2) from [46] about the degradation coefficients in specific conditions (i, T, and RH). In the present paper, the computation of the degradation mechanisms is explained briefly, for more detailed information, the authors describe this model in [41].

As stated by the DoE in [47], the voltage drop represents an appropriate way to measure the degradation of a stack. The lifetime of an FC stack is considered ended when there exists a voltage drop of 10% or more from its nominal value. This can be measured with the degraded ratio, which is shown in Eq. (8). As a starting point to understand the way in which degradation has been computed, it is essential to know that the developed degradation model estimates the FC degradation rate based on the evolution of the current density, the stack temperature and the average relative humidity in the FC stack.

$$\delta = 1 - \frac{V_{deg}}{V_{FC}} \tag{8}$$

The data obtained from [46] is adjusted to obtain some reference degradation ratios (Table 2). These values can be used to model the degradation ratio that allows the calculation of the degradation of the stack. The degradation ratio depends on the operating conditions and electrochemical phenomena taking place on the stack and this is calculated by using expression (9).

$$\delta = \int_0^t \left[\frac{d\delta}{dt}\Big|_{lp} + \frac{d\delta}{dt}\Big|_{lc} + \frac{d\delta}{dt}\Big|_{hp} + \frac{d\delta}{dt}\Big|_{nt} \right] dt + \frac{d\delta_{ss}}{dn_{ss}} n_{ss} \tag{9}$$

The previous equation (Eq. (9)) shows how the operation of the FC influences degradation. The degradation sources included in the equation can be divided into: low-power (lp), load-change (lc), high-power (hp), medium-power or natural (nt), and start-stop (ss). However, the values in Eq. (9) are not the ones listed in Table 2, they are scaled to consider the electrochemical phenomena and operating conditions of the stack. This scaling process is done by using the list of expressions presented below (Eqs. (10)–(14)).

$$\frac{d\delta}{dt}\Big|_{lp} = \frac{d\delta}{dt}\Big|_{lp,ref} \cdot \xi_{lp}(i) \cdot \tau(T) \cdot \eta\left(\overline{RH}\right) \tag{10}$$

$$\frac{d\delta}{dt}\Big|_{lc} = \frac{d\delta}{dt}\Big|_{lc,ref} \cdot \xi_{lc}(i) \cdot \tau(T) \cdot \eta\left(\overline{RH}\right) \tag{11}$$

$$\frac{d\delta}{dt}\Big|_{hp} = \frac{d\delta}{dt}\Big|_{hp,ref} \cdot \xi_{hp}(i) \cdot \tau(T) \cdot \eta\left(\overline{RH}\right) \tag{12}$$

$$\frac{d\delta}{dt}\Big|_{nt} = \frac{\frac{d\delta}{dt}\Big|_{hp,ref} \xi_{hp}(i_{hp}) - \frac{d\delta}{dt}\Big|_{lp,ref} \xi_{lp}(i_{lp})}{i_{hp} - i_{lp}} (i - i_{lp}) + \frac{d\delta}{dt}\Big|_{lp,ref} \xi_{lp}(i_p) \tag{13}$$

$$\frac{d\delta_{ss}}{dn_{ss}} = \frac{d\delta}{n_{ss}}\Big|_{ref} \tag{14}$$

The scaling function ξ is used to model the effect of electrochemical phenomena in the degradation process. This value depends on the current density. In addition, the known experimental information [46] allows establishing some current degradation limits of 1 and 0.33 A/cm^2, i_{hp} and i_{lp} respectively. This electrochemical degradation can be explained in further detail by using the expressions that model it (ξ).

At low power, the electrochemical degradation is controlled by ξ_{lp}, which is shown in Eq. (15). Considering the known data from [46], this parameter has a value of 1 at 0.01 A/cm^2. In these conditions, the decay in the FC performance comes from a change in the fluoride release rate (FRR) [48] and a carbon corrosion of the catalyst surface.

$$\xi_{lp} = -0.176 \cdot \ln i + 0.169 \tag{15}$$

The case of high power degradation is more intuitive, degradation comes from the high temperatures produced in the stack. As the temperature of the stack is related to its current, this expression can be modeled as shown in Eq. (16).

$$\xi_{hp} = \frac{i}{i_{hp}} \tag{16}$$

Furthermore, not only do low and high currents act upon the degradation mechanisms, but the load-change level also represents a significant factor in this process. The driving cycle conditions and EMS lead to the choice of the dynamic performance of the vehicle (di/dt), how this load-change influences degradation (ξ_{lc}) can be computed by considering the reference ξ_{lc}, that comes from a reference current step. The value of ξ_{lc} can be modeled considering the change in the current step as shown in Eq. (17).

$$\xi_{lc}\left(\frac{di}{dt}\right) = \frac{|\Delta i|_{dt}}{2\,|\Delta i|_{ref}} \tag{17}$$

When working to produce a medium power level, degradation comes from the continuity of low and high power degradation mechanisms. Thus, a special parameter to compute this degradation is not needed, as shown in (13). In these conditions, degradation is mainly caused by the voltage decay of the stack, which is why it is called natural degradation.

Furthermore, the current produced by the stack is not the only factor influencing degradation. The operating conditions of the stack are also an important factor. It has been proven [46] that there is a relation between fluoride release rate change and temperature. Also, platinum dissolution mechanisms, which cause electrochemical surface area (ECSA) decrease, are related to the temperature increase [49]. These temperature relations with degradation allow to design the expression shown in Eq. (18) to model this degradation effect.

$$\tau(T) = -5.390 \cdot 10^{-4} T^2 + 0.399 \cdot T - 71.576 \quad \forall T \in [310, 373.15] \tag{18}$$

Beside temperature, relative humidity (RH) also has an impact in the degradation process. Humid conditions favor the growth of Pt grains and this is related to ECSA decrease rate. In [50] voltage cycling degradation tests allowed to obtain experimental data about this phenomena, which leads to the equation shown in (19).

$$\eta(RH) = 0.10646 \exp^{0.028 \cdot RH[\%]} \tag{19}$$

The present model has been validated by using data from the operation of a real FC bus [46] and simulating real driving cycle conditions of its daily routes [41,51]. The later comparison of the simulation results

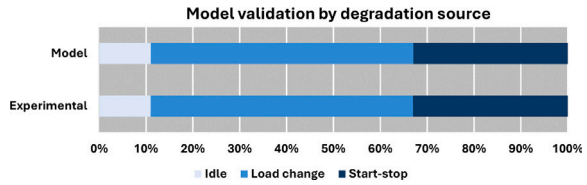

Fig. 5. Error between the experimental and simulation values in the validation of the degradation model [41].

and the experimental data shows an error lower than 0.1%, which is significantly low. The computed degradation sorted by its generation source for each case can be seen in Fig. 5.

These results lead to an accurate model which can be considered appropriate for its integration into the current simulating tool. The integration of the present model in the developed simulation tool can be done due to the dynamic nature of the degradation model. As this model includes the current, dynamics and conditions of the FCS at each time step, matlab-Simulink is used to feed this data into the degradation model and compute the final voltage decay. The values of the parameters introduced in the model equations come directly from the performance of the FCS. The assumptions about high and low current are based on standard values for a vehicle FCS. Additionally, the start-stop degradation parameter has been defined to simulate that the vehicle has a stop every two cycles, which is considered appropriate for the interurban use of the LCV.

2.4. Driving conditions

The present study aims to understand the particularities of the performance of an LDFCV. For this purpose, the correct modeling of the vehicle performance is important. However, being able to reproduce realistic driving conditions which are representative of a typical LCV mission, is a key factor in the simulation process. For this kind of road vehicle any analysis, such as emission or consumption, follows the WLTP protocols. These procedures are divided into different WLTC cycles depending on the power-to-mass ratio (PMR) of the vehicle. As the PMR varies depending on the propulsive system, different driving conditions should be tested. In this case, the 120 kW e-motor provides a high PMR which is capable of working under the power demanded by the WTLC3b cycle. However, for the small e-motor, the conditions proposed by the WLTC2 cycle are more suitable.

In addition, when choosing the driving conditions that are appropriate for any vehicle, it is important to think about its usual mission. LCVs are quite versatile and used by the consumer for many different purposes. A frequent purpose for an LCV is the delivery sector. This application, in terms of driving conditions, is compatible with the WLTC2 cycle, because this represents an urban mission. However, this specific use may also require long journeys to the delivery center, which means an interurban use of the van. In addition, the use of camperized vans for leisure purposes has increased in the last few years. This interurban use of the LCV is more similar to the WLTC3b driving conditions.

In conclusion, both the WLTC3b and the WLTC2 represent conditions that are appropriate for an LCV and they are both simulated in the present paper due to the importance of understanding the performance of the vehicle under its different possible missions.

2.5. Development of the simulating tool

The designed simulation platform includes all the previously explained models. However, its integration to generate a virtual vehicle is not trivial. Since the EMS chooses the best possible current density for the desired optimal performance, some information about the performance of the present FCS is needed. For this purpose, the FCS model is operated under a wide range of operating conditions that are appropriate for the working vehicle. The current demand to the system in this case is a standard polarization curve. Before the polarization curve, a small warm-up procedure is performed so that the temperature of the stack is stable. In this way, the system is characterized for a wide set of stack operating conditions (T and P).

These simulations provide a set of data outputs that are fed to the EMS. In this way, considering the conditions of the system and the specifications of the powertrain, the EMS selects the optimal value in terms of the cost (as explained in Section 2.2). Simulink is a powerful platform for this kind of simulations because it allows to compute the value of current density in real time and considering the outputs calculated by the FCS.

3. Results and discussion

The present section aims to analyze in detail the data obtained from the performed simulations and compare the studied LCV architectures to understand the advantages and disadvantages of each configuration. To achieve this primary objective, the results can be divided into the study of the performance, the durability of the FCS and the suitability for the typical LCV mission.

3.1. Analysis on FC-powered LCV performance

The performance of a vehicle comes from the analysis of the parameters that are considered critical for its driving. The performance of a passenger car is established by its fuel consumption and range. Additionally, these two values would allow to compute the energy consumption of the vehicle, which provides relevant information as the present vehicle is a hybrid van which uses both H_2 and electricity. Nevertheless, the case of a commercial vehicle is different because its load capacity also needs to be considered. The cargo capacity of the LCV depends on the chosen powertrain architecture which is related to its driving conditions. However, this will be studied in detail in Section 3.3, which analyses the different kind of missions for this vehicle. Therefore, the present section can be divided into three different topics: H_2 consumption, range and energy consumption.

3.1.1. H_2 consumption

The consumption of a vehicle is usually related to the range it is able to achieve. However, since the proposed architectures are hybrid vehicles, the relation between these values is not simple. As explained in Section 2.2, the power demanded by the driving conditions is split between the electric battery and the FCS. This EMS selects the power distribution that allows the FCS to consume the optimal amount of H_2.

The simulations that have been carried out can be divided into 4 different sets, two depending on the driving conditions and another two depending on the H_2 tank of the vehicle. Firstly, the WLTC3b cycle represents an interurban mission, thus, more aggressive driving conditions in terms of load and dynamics. The results of these simulations are shown in Figs. 6 and 7 and are representative of a charge-sustained operation.

Fig. 6 shows an area of the surface that has no available results. The reason behind this is that it is not possible to drive the specified vehicle under the proposed conditions for that architecture. This powertrain design consists of the 30 kW FCS coupled with a small battery of 1.6 kWh, thus, the provided power is not enough to meet the demand of the cycle.

It is important to remark that consumption represents the amount of H_2 used from the tank. Since the architecture of the vehicle has a maximum amount of this gas that can be consumed, this value is expressed by kg used by the vehicle per 100 km (kg/100 km).

Figs. 6 and 7 show how the amount of H_2 consumed is lower as the size of the FCS increases. A bigger FCS provides the desired power by working under lower current densities, which allows a performance

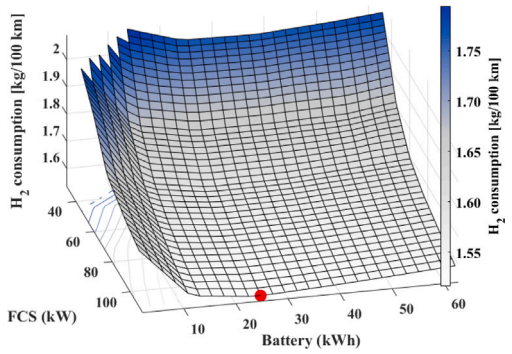

Fig. 6. H_2 consumed in the WLTC3b driving conditions with a 4 kg H_2 tank.

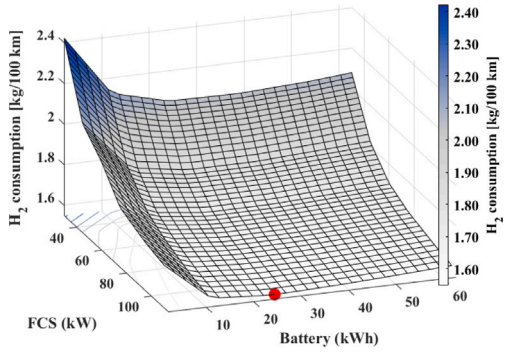

Fig. 7. H_2 consumed in the WLTC3b driving conditions with a 6 kg H_2 tank.

that is closer to idle conditions. The work under lower currents leads to a higher efficiency in the polarization curve and, thus, a smaller H_2 consumption.

In these figures, the influence of the battery size can also be noted. The increment in the size of the battery produces an increase in the weight of the vehicle, which leads to a higher power demanded and a larger amount of H_2 consumed required by the LCV. When looking at the size of the battery axis it is significant to note that its influence is not linear. The brake-recovery power battery (1.6 kWh) leads to an important increase in the H_2 consumption because in that design the FCS is the only source of power. From the 10.5 kWh battery, the influence of its size is smaller. In Figs. 6 and 7, the minimum H_2 consumption design is marked in red.

When calculating the difference between the obtained consumptions in each architecture and the optimal one, the results are significant. The architectures with a 4 kg tank (Fig. 6) show a maximum difference of 30% and the ones with a 6 kg tank have a variation up to 50%. In the plotted results, it is also interesting to see that the variation is not linear and there is a quite large area in which the difference stays below 8%. The powertrain designs that are close to this optimal point have FCS with higher power than 60 kW and a battery larger than the one providing 20 kWh, around 25 kWh.

This can be explained by considering not only the weight added by the battery but also taking a close look at the power distribution made by the EMS (Fig. 8). When comparing the current production of a set of powertrains with the same battery and different FCS, it can be seen that the current is very different. The steady current level is much larger for the smaller FCS than for the bigger ones. Thus, the larger FCS works under more efficient conditions and can consume less H_2 to fulfill the needs of the system.

In this plot (Fig. 8A), it can also be noted that the current difference becomes smaller when the FCS has a maximum power higher than 75 kW. Therefore, in Figs. 6 and 7, there is a small variation area in those architectures. The second part of this (Fig. 8B) shows the power distributions, which is also an interesting matter. The power provided by each FCS is different depending on its maximum. The FCS with higher maximum power have more dynamic performances and adapt to the power peaks demanded by the cycle. When the FCS is small, it works more steadily while the battery absorbs the power peaks. This steady performance also means a higher steady power to charge the battery that is being constantly used.

The second kind of mission, represented with the WLTC2 cycle, can also be studied (Figs. 9 and 10). Firstly, in this case, it is important to note that some values are not represented in the figures. The reason behind this is that the power demanded by the cycle is too low and those designs were not able to meet the SOC of the battery and ended up overcharging it.

In the presented (Figs. 9 and 10) the observed trends are the same as in Figs. 6 and 7 that represent the WLTC3b driving conditions. The presented figures show that the consumption is higher in the WLTC3b driving conditions as expected because these imply a higher power demand. However, the difference between the minimal consumption of the WLTC3b to the WLTC2 conditions is only 10%.

Additionally, from Fig. 10 is important to remark there is a consumption peak which comes from the use of a high FCS and a low-power battery. The WLTC2 consumption results show that, in this case, the optimal design is composed of a 12 kWh battery and a high-power FCS. As in the WLTC3b obtained data, the presented plots show that there is a region in the design space for which the variability is low. The present driving cycles are optimized for a large FCS (>65 kW) and a small battery (10–20 kWh).

Finally, the different tank sizes can also be compared from the set of obtained results. They show that the difference in the H_2 consumption does not change significantly with the size of the fuel tank. A larger H_2 tank implies around a 1% more of H_2 consumed. This difference comes from the weight increase of the vehicle.

Finally, it is important to remark that understanding the minimum consumption point is essential when establishing the architecture of the vehicle. However, from this results section, it is more important to have a global understanding of the consumption distribution, which is given by the study of several different designs than to select a specific optimal architecture. The final architecture could depend on more design aspects such as cost or environmental impact and cannot be chosen considering only one of them.

3.1.2. Range of the vehicle

In the studied cases, the range of the proposed vehicles is highly dependent on the performance of the FCS. The chosen energy strategy is charge depleting at first, and then, charge sustained for the electric battery around 0.25 of the SOC. Thus, this energy source is used until its state of charge reaches a value of 0.25, after that, the FCS is combined with it to maintain its SOC by using the existing EMS.

The range provided by the electric battery to the vehicle is easy to calculate considering the explained energy management. The driving conditions are simulated until the SOC reaches the desired value. Afterward, the implemented simulating tool (Section 2) is used to compute the range of the vehicle the FCS provides. As expected, the range provided by the electric battery is proportional to its energy content.

The addition of the battery and H_2 autonomies provides the value of the total range of the vehicle, which is shown in Fig. 11C and D for the 4 kg and 6 kg H_2 tank respectively and the WLTC3b driving conditions. From these two figures, it is important to note the high autonomy of the vehicle at the maximum point. This maximum is very different depending on the H_2 tank, in contrast with the consumption results. The difference between the autonomies provided by each tank is constant and around 110 km which represents a 20% deviation from the maximum possible value (obtained with the 6 kg tank architecture).

Fig. 11C and D show the total range of the vehicle. However, it is also interesting to study in an isolated way the H_2 range, in other

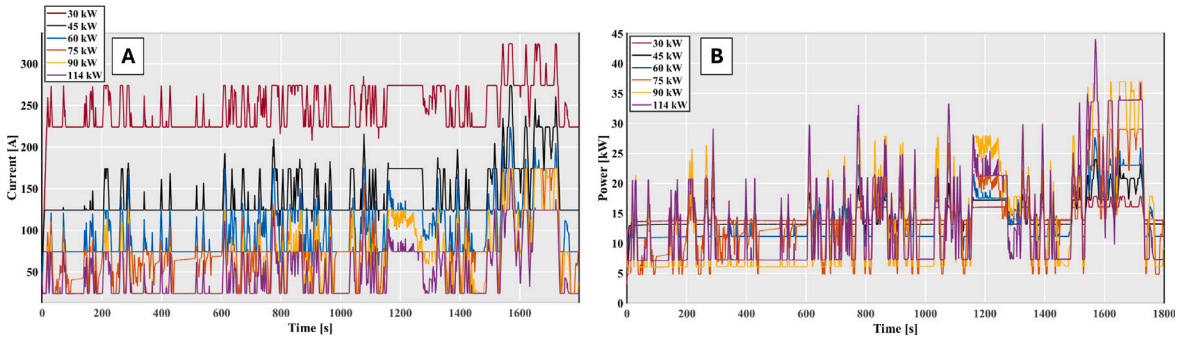

Fig. 8. Current and power distribution for a 20 kWh battery and variable FCS.

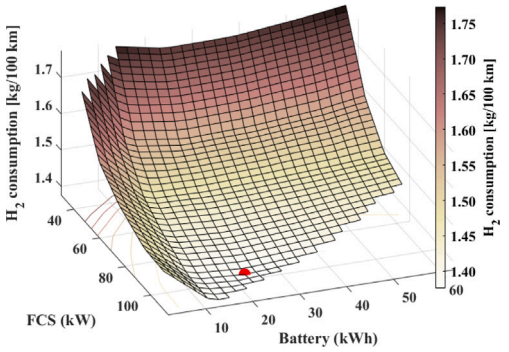

Fig. 9. H_2 consumed in the WLTC2 driving conditions with a 4 kg H_2 tank.

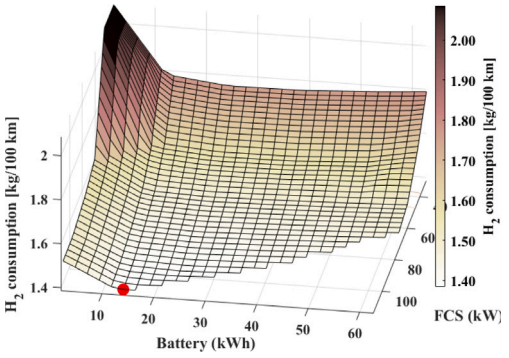

Fig. 10. H_2 consumed in the WLTC2 driving conditions with a 6 kg H_2 tank.

words, the range achievable in charge-sustaining mode with the FCS producing most of the power required by the e-motor, presented in Fig. 11A and B. As expected, the size of the FCS increases the possible autonomy.

Additionally, it can be noted that increasing the size of the battery also has an impact on the H_2 range. This influence is higher at small battery sizes. This is related to the results seen in Section 3.1.1 about a higher H_2 consumption motivated by the increased weight as the battery capacity increases. The quantification of the difference from the maximum H_2 range, shows the same phenomena as in the H_2 consumption. There exists a wide area of the plotted surface in which there is a small variation around 5% from the maximum H_2 range design. This similar results zone is marked by FCS of more than 75 kW and batteries bigger than 12 kWh. Out of this region, smaller FCS decrease the range gradually and can make a difference up to 35% when using a H_2 tank of 6 kg and 25% with the 4 kg tank. In both cases, the range distribution with the different powertrain designs follows the same trend.

The WLTC2 driving conditions are presented in 12 and show the same tendencies in the results. The lower power demand of this cycle allows a lower H_2 consumption (Section 3.1.1) and a higher range of the vehicle. In this cycle, as H_2 consumption is lower, the difference in performance produced by the size of the H_2 tank becomes more important. A difference in 2 kg of fuel from the tank represents a variation of 32% to the maximum possible range using only H_2.

Additionally, Fig. 12C and D show the total range of the vehicle. As expected, the vehicle range increases in the WLTC2 compared to the WLTC3b. In this driving condition, the 2 kg fuel difference between architectures produces a 132 km change, which is around a 24%. The main reason behind this is that the lower dynamics and loads allow a better utilization of the H_2 fuel.

Finally, Fig. 13 shows the amount of range that is produced from H_2 respect to the total range of the vehicle. Each of the 4 different graphs show the same trend, the influence of H_2 in the total range grows as the battery is smaller, as expected. When the H_2 tank is bigger, the relative impact on the total range also increases. The size of the FCS also has an influence on the H_2 range with respect to the total. However, the increase of the FCS can produce around a maximum 10% of change in the range with respect to the total, and the battery size can produce a difference higher than 80%. This allows to understand the high importance of the battery choice on the range of the vehicle.

From Fig. 13 it is also interesting to note that the minimum values are around 55%. This shows that the main energy source of the studied vehicles is the FCS. The electric battery is used to support the FCS to accomplish the LCV mission in the most efficient way.

In the analysis of the battery influence on the range of the vehicle, it is also important to comment the weight of the battery. The change from a small to a large battery can add up to 400 kg in the presented architectures. This represents around a 16% increment in the total weight of the LCV. The weight increase has a negative impact on the lifecycle emissions and cost of the vehicle, but, in the case of an LCV, it also influences its load transportation capability.

3.1.3. Energy consumption

Once the range of the vehicle and its fuel consumption have been studied, it is also interesting to study its energy consumption. The proposed architectures are hybrid electric vehicles, thus, the electricity consumed is also an important matter in its performance. The energy consumed by the vehicle can be computed as shown in (20).

$$E_{cons} = \frac{Batt_{capacity} + LHV \cdot m_{H_2}}{range_{total}} \tag{20}$$

The obtained results about the energy consumption of the vehicle architectures in each conditions are shown in Fig. 14. This figures show that the minimum consumption is obtained for the highest battery and FCS sizes. The reason behind this is that this allows both systems to work under low current densities and be more efficient. It can be noted that when the battery size increases, the energy consumption decreases faster than when the FCS maximum power increases. Therefore, the performance of the battery is more efficient than the FCS.

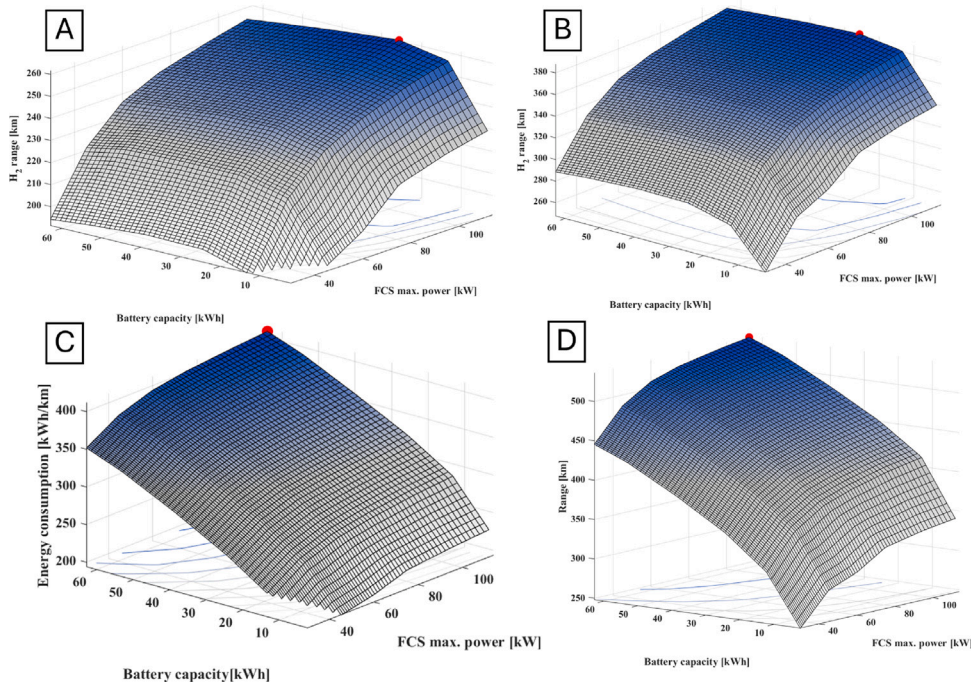

Fig. 11. A. Range provided by the FCS in the WLTC3b cycle for the architectures with a 4 kg H_2 tank. B. Range provided by the FCS in the WLTC3b cycle for the architectures with a 6 kg H_2 tank. C. Range of the vehicle in the WLTC3b cycle for the architectures with a 4 kg H_2 tank. D. Range of the vehicle in the WLTC3b cycle for the architectures with a 6 kg H_2 tank.

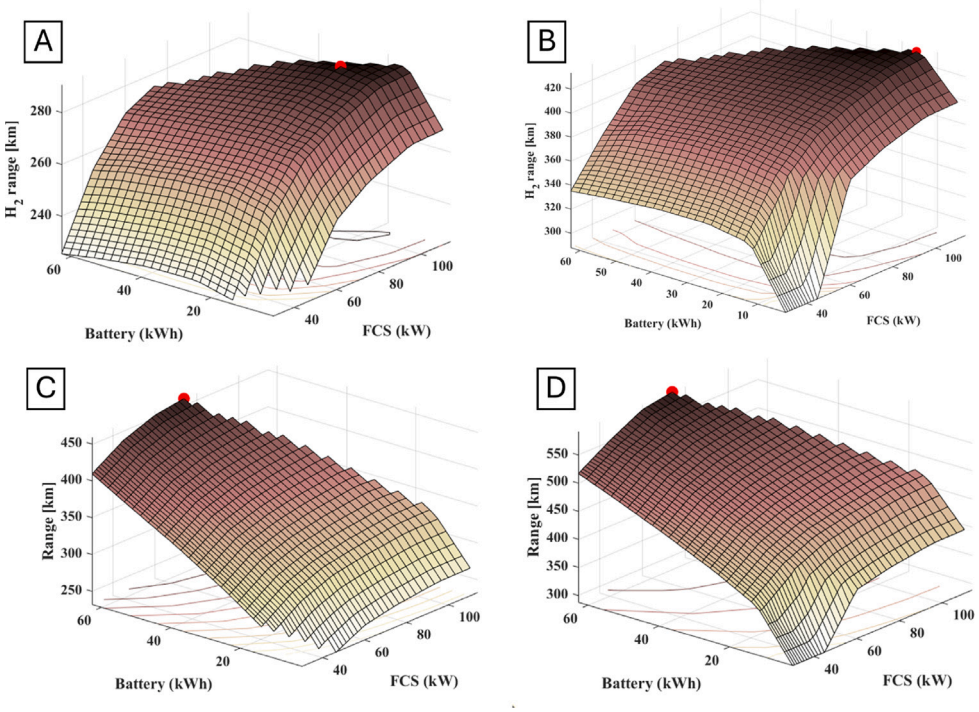

Fig. 12. A. Autonomy provided by the FCS in the WLTC2 cycle for the architectures with a 4 kg H_2 tank. B. Autonomy provided by the FCS in the WLTC2 cycle for the architectures with a 6 kg H_2 tank. C. Autonomy of the vehicle in the WLTC2 cycle for the architectures with a 4 kg H_2 tank. D. Autonomy of the vehicle in the WLTC2 cycle for the architectures with a 6 kg H_2 tank.

However, from these figures, the essential conclusion is that there exist a set of architectures, from higher than 60 kW FCS and higher than 30 kWh in which the change energy consumption is very small.

To sum up, from the present section it is important to remark that the size of the H_2 tank has an insignificant influence on the H_2 consumption of the vehicle (~1%) in exchange for an important increase in H_2 range (up to a 32%). Additionally, it has been proved that the

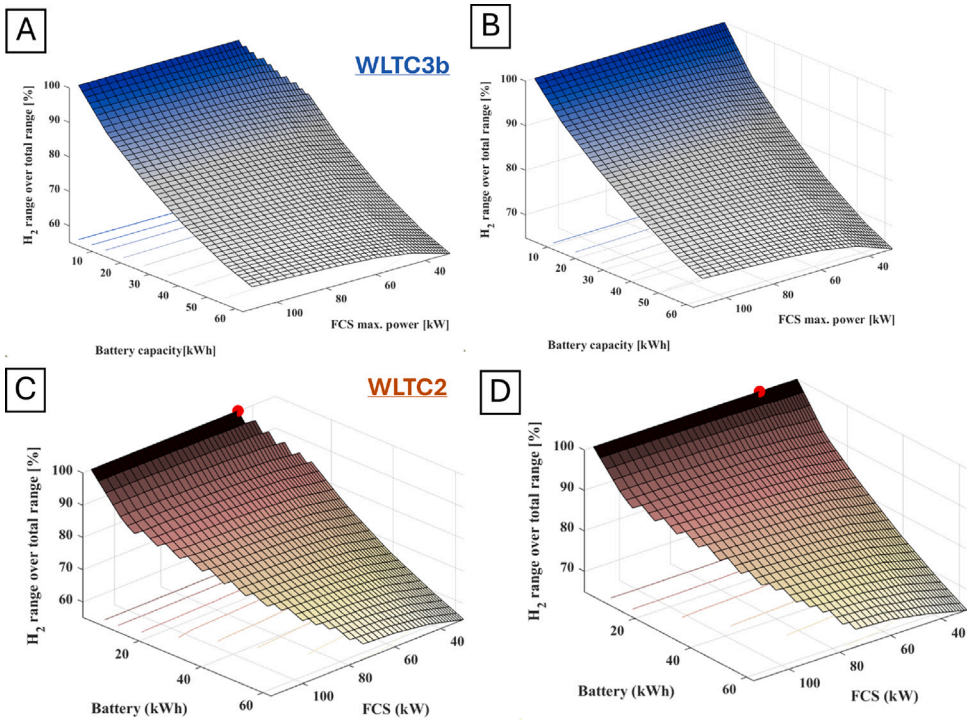

Fig. 13. A. Percentage of the range provided by the FCS respect to the total range of the vehicle in the WLTC3b cycle for the architectures with a 4 kg H_2 tank. B. Percentage of the range provided by the FCS respect to the total range of the vehicle in the WLTC3b cycle for the architectures with a 6 kg H_2 tank. C. Percentage of the range provided by the FCS respect to the total range of the vehicle in the WLTC2 cycle for the architectures with a 4 kg H_2 tank. D. Percentage of the range provided by the FCS respect to the total range of the vehicle in the WLTC2 cycle for the architectures with a 6 kg H_2 tank.

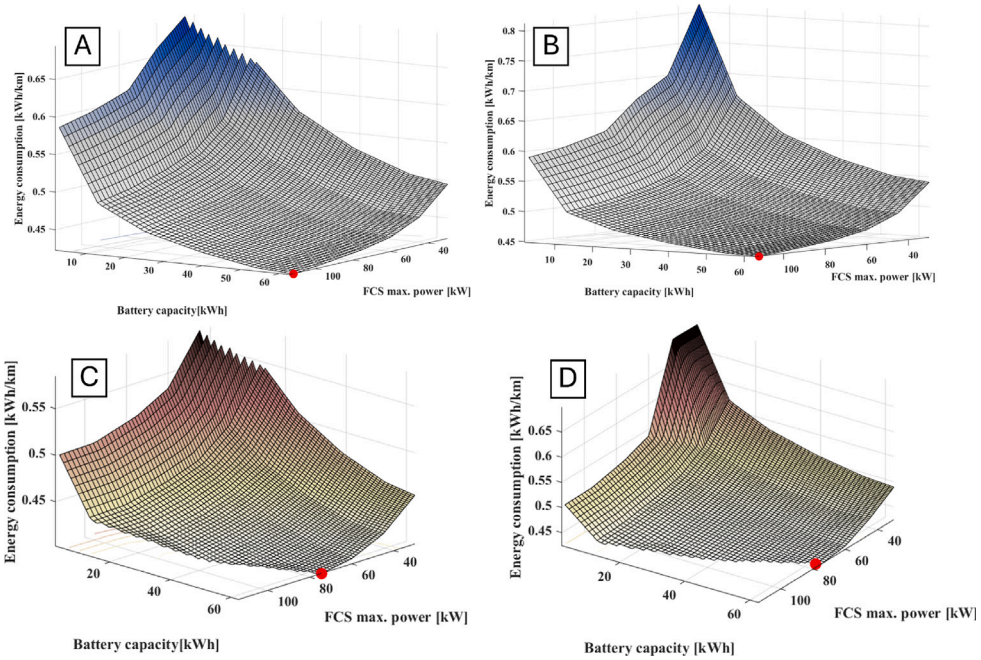

Fig. 14. A. Energy consumed by the vehicle in the WLTC3b cycle for the architectures with a 4 kg H_2 tank. B. Energy consumed by the vehicle in the WLTC3b cycle for the architectures with a 6 kg H_2 tank. C. Energy consumed by the vehicle in the WLTC2 cycle for the architectures with a 4 kg H_2 tank. D. Energy consumed by the vehicle in the WLTC2 cycle for the architectures with a 6 kg H_2 tank.

range of the vehicle is highly dependent on its driving conditions and fuel tank. In the WLTC3b case, the powertrain architecture can increase the range of the vehicle up to a 116% with the 6 kg H_2 tank and a 112% with the 4 kg tank. However, in the WLTC2 driving conditions, the 6 kg tank can produce a 96% increase in range while the 4 kg tank can only achieve a 86% increment. Thus, the definition of the typical LCV mission is crucial in the choice of the powertrain of the vehicle.

3.2. FC durability evaluation for LCV architectures

In the evaluation of an FCS-based powertrain, performance, and range are significant factors that must be considered. However, this

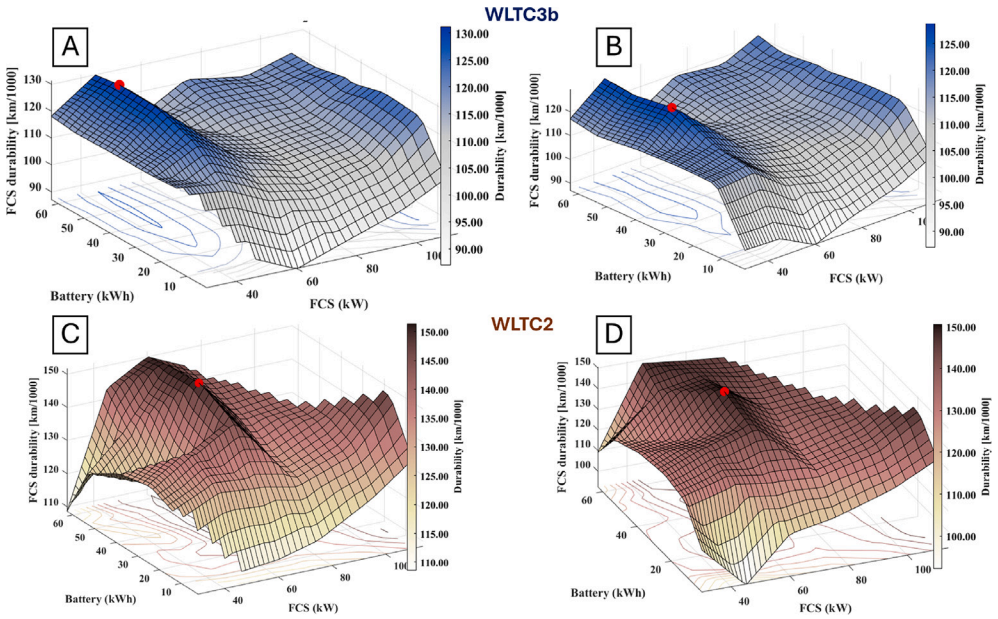

Fig. 15. Durability of the FCS. A. Powertrain architectures with a 4 kg H_2 tank for WLTC3b driving conditions. B. Powertrain architectures with a 6 kg H_2 tank for WLTC3b driving conditions. C. Powertrain architectures with a 4 kg H_2 tank for WLTC2 driving conditions. D. Powertrain architectures with a 6 kg H_2 tank for WLTC2 driving conditions.

kind of technology has a particular parameter that needs to be studied in detail: its durability. As it has already been commented in Sections 1 and 2.3, different phenomena trigger degradation mechanisms affecting the MEA of the FC stack and may cause a decay in the cell voltage. Therefore, the durability of the FCS is a key aspect to study, particularly in automotive applications in which the FCS may be subjected to high-dynamics conditions. A fast degradation of the system may result in the requirement of a high amount of replacements during the usual lifetime of a given vehicle, particularly when the expected vehicle lifetime is high. This would result in an important increment in the cost and emissions along its life cycle. Fig. 15 shows the durability of the FCS in each of the different architectures for the considered driving cycles. The durability value was calculated considering the end of life when the stack voltage decreases by 10% in the reference condition of 1 A/cm^2. From the presented plots, it is interesting to note that the evolution of this parameter does not show a clear trend with the size of the FCS or the electric battery since it depends on how the EMS manages them in terms of dynamics. Nonetheless, the four cases that are being discussed exhibit trends that are rather comparable in terms of the durability of the FCS. The 4 graphs displayed in Fig. 15 show that the maximum lifetime of this power generation system is reached for a medium-size FCS. Nevertheless, the FCS size of the optimal case is different in each scenario.

The understanding of the durability of the system passes through a detailed analysis of each degradation source. As explained in Section 2.3, the voltage drop comes from a membrane and catalyst decay that is produced by different phenomena. The most important sources of degradation that are studied to understand the tendencies in Fig. 15 are high-power, load-change, natural, idle, and start-stop degradation. The voltage drop produced by each of these sources has a different influence on the energy production capability of the FC, being the highest effect attributed to load-change degradation. A deeper analysis of the dynamics of each different powertrain design shows that to obtain the least consumption performance, the power split of each design are different and this influences the current supplied to the FCS and, thus its durability. As expected, a high level of dynamics increases the load-change degradation level, which has an important impact on the shape of the durability curve. Nevertheless, the influence of other degradation mechanisms is also important and should not be neglected.

From the results obtained with different driving cycles, it is interesting to note that the maximum durability of the FCS is obtained for the WLTC2 cycle, as expected due to its lower dynamics and maximum load. Additionally, it is interesting to note that the 6 kg tank provides higher durability than the 4 kg tank design. The same effect is observed in the WLTC3b cases. However, the difference does not go over a 3% and it can be considered a minor impact. Additionally, the difference in durability of the suboptimal designs compared to the design offering maximum FC lifetime is significantly higher in the WLTC2 cycle, compared to the WLTC3b cycle. The results show that in the lower dynamics cycle, the influence of load-change degradation is higher. An increment of 2 kg in the tank changes the voltage drop produced by load-change degradation from 60% to 77% of maximum difference between architectures. Besides, in a higher dynamics case as the WLTC3b, this H_2 increment only produces a change from 65% to 67% from the optimal case. The stability in the results may be a benefit of the smaller H_2 tank in the decision of a vehicle architecture.

Fig. 15A and B show that the maximum durability for the WLTC3b conditions is obtained for a 45 kW FCS and a 45 kWh battery. Nevertheless, Fig. 15C and D show a maximum in the 60 kW and 33 kWh design for the WLTC2 cycle.

The variability of the results depends on the studied case. The possible change in the durability of the system when working under WLTC2 conditions has a maximum of 25% for the 4 kg tank and 36% for the 6 kg tank. In contrast, when driving under WLTC3b conditions, the maximum variation in durability is around a 33%, independent of the size of the fuel tank. The understanding of the variability of the results in each case will allow the decision of the optimal powertrain design for the chosen vehicle mission. The analysis of the durability and its evolution depending on each architecture is a significant matter that will allow to understand how to reduce the cost of the vehicle or the lifecycle related emissions in future research activities.

3.3. Influence on the LCV mission

The main objective of the present paper is to analyze the influence of the different proposed powertrain architectures for its use in an LCV. For this purpose, the mission or typical use of this kind of vehicle needs to be defined. As vans are currently used for several applications, it is important to remark that this paper focuses on their commercial use (delivery, transport of goods or equipment...) [52]. The typical mileage of use in a year of this kind of vehicle can reach up to 50,000

miles, which means that its typical use during a day can be around 320 km [53]. Considering that delivery can also take place in rural areas which are further away from each other and other factors such as traffic may influence this value, the maximum mileage per day established is around 250 miles or 400 km.

This information and the previously analyzed results allow the optimal propulsion system architecture selection for the desired vehicle. This LCV should provide the highest FCS durability, as well as the lowest H_2 consumption and maximum range of around 400 km [54]. The first decision that can be made is about the fuel tank. The H_2 tank of 6 kg shows a consumption insignificant increase of 1% with respect to the 4 kg tank, as well as a 1.5% durability decrease. However, the exchange for these two minimal disadvantages is an increment of almost 50% of the H_2 range, which translates into 30% more vehicle autonomy. Therefore, an amount of 6 kg of H_2 is selected for the recommended powertrain.

This known, the most important factor to maximize is the durability of the FCS. This value will establish the number of replacements of the FCS that will be needed during its lifetime, which is a maximum of 240,000 km for an LCV [55]. The versatility of these vehicles, which can both operate under WLTC2 and 3b driving conditions, leads to a compromise in the choice of durability. The comparison between the two maximums allows to narrow the choice of the architectures for a propulsive system using a 33 kWh electric battery and an FCS between 45 kW and 60 kW. The 60 kW FCS provides the best durability for urban driving conditions, whereas the 45 kW FCS would be better for rural delivery or interurban use of the van.

It is also interesting to note that reducing the size of the battery up to 20 kWh does not have a high impact on durability and it reduces consumption, which may influence costs and lifecycle emissions. Thus, in future studies that consider Total Cost of Ownership (TCO) and Life Cycle Assessment (LCA), the presented optimal points could be revised.

Finally, the study of consumption allows to make the final decision. This parameter shows that the 60 kW FCS would increase consumption by 8% from the optimal case in WLTC3b conditions. Nevertheless, the 45 kW would imply a 14% increment. The influence in the WLTC2 cycle is lower but following the same increasing trend. This information is particularly important for a scenario in which H_2 production entails high costs or lifecycle emissions, as in this case, the best solution would imply a higher power FCS.

Since LCVs are mainly used in urban environments, the design that optimizes durability for this kind of conditions (WLTC2) and allows a compromise in H_2 consumption is chosen as the final recommended powertrain design, provided that other aspects such as cost or environmental impact may influence this selection.

To sum up, the performed study allows to understand how different sizes of the powertrain components influence the performance and durability of the system. Additionally, this analysis shows that for a typical LCV, a powertrain architecture composed of a 60 kW FCS, a 33 kWh electric battery, and a 6 kg H_2 tank provides performance and durability benefits while meeting the requirements of use for its typical driving conditions.

4. Potential for industrial applications

Given that FCS technology is currently in advanced stages of development with high TRLs, the findings of this study hold substantial relevance within the current industrial framework. The key finding of this study lies in the comprehension of how different sizing combinations in the propulsive system impact LCVs. This information would be of high interest for the LCV manufacturers that are currently working on the development of their vehicle prototypes.

The relevance of the performed analysis comes from the novelty of the used methodology (Section 2), which has been calibrated with real experimental data and, therefore, provides realistic information about the operation of a FCV.

As detailed in Section 1, there exists a knowledge gap in the LCV sector regarding the optimal FCS-based powertrain architecture for achieving decarbonization in this industry. The present manufacturers in this market sectors have proposed very different powertrain solutions, but it seems to be unclear which would be the optimal one. The current paper presents a proposed powertrain suitable for this vehicle category. This finding sheds some light into the current state of the art knowledge gaps. The meticulous level of detail employed in the simulation campaign enables any company to tailor the design to meet the specific requirements of its vehicles, provided they share the architecture of a van and have a mission of use similar to the ones simulated in the paper.

Moreover, the diverse range of architectures simulated in this study enables LCV manufacturers to analyze various LCV missions beyond the scope of this paper, such as recreational or leisure vans, private or domestic non-business use, and transportation of goods or equipment [52]. For example, if the van manufacturer focuses on the commercialization of camperized vans used for leisure purposes, it would make sense to maximize the range of the vehicle mainly in WLTC3b driving conditions, which would be more appropriate for this vehicle mission. However, delivery van users would rather focus on maximizing durability of the FCS rather than range. The reason for this is that vehicles used for these types of applications typically cover shorter distances, so the owners want to maximize the van's cost-effectiveness.

The dataset obtained regarding performance and durability stands as highly valuable in its own. However, companies specializing in LCV manufacturing possess a significant level of expertise regarding the implications of producing LCVs. Consequently, a vehicle manufacturer could utilize this data to accurately assess the cost and lifecycle emissions of the vehicle and evaluate the tested architectures from a commercial point of view, thus accelerating the vehicle development process since the preliminary powertrain design could be selected directly.

The companies involved in the design of LCVs could use the obtained datasets that have been plotted into result maps to understand the way in which the architecture of the powertrain influences the final characteristics of the vehicle, as it has been done in the present research paper, but using the specific architecture of a real vehicle. Additionally, they could use these data maps to generate cost maps, as they know their vehicle assembling, manufacture or fuel costs. The obtained data would be extremely helpful in the preliminary design phase of a vehicle, as it would allow to evaluate virtual vehicles and accelerate the design process.

In conclusion, this study has an important potential for the industrial application of FCS technology applied to LCVs. The insights gained are relevant for manufacturers engaged in prototyping activities of this kind of vehicle. The methodology, calibrated with real data, addresses critical knowledge gaps and offers flexibility for testing different powertrain designs. Moreover, the diverse range of simulated architectures extends applicability, providing insights into various LCV mission requirements. The dataset obtained will be even more valuable, complemented by the expertise of manufacturers in assessing cost and commercial viability, highlighting the potential of FC-powered LCVs for decarbonization in the automotive sector.

5. Conclusion

The present study has successfully generated results about the performance and durability of the studied FC-based powertrain architectures for LCV applications. The obtained set of data is highly valuable in the current research framework, as it allows to have a better understanding about how the different sizes in the components of the powertrain influence the specific performance of an LCV in terms of H_2 and energy consumption, range and durability.

The analysis of the results leads to the obtention of the following conclusions:

- The H_2 consumption of an LCV exhibits an inverse relationship with the size of the FCS. Optimal consumption levels are achieved with the largest FCS configuration, coupled with a medium-sized electric battery. Thus, the optimal propulsion system architecture in terms of H_2 consumption would have a maximum FCS power of 114 kW and a battery capacity of 20 kWh for WLTC3b conditions and 10.5 kWh for the WLTC2 cycle. This configuration enables the FCS to operate at a efficiency level during its typical mission. Consumption remains relatively stable for medium or large FCS sizes. However, employing a small FCS would necessitate higher current density, thus, reduced efficiency in the polarization curve, and a notable increase in fuel consumption, up to 50% in the most adverse scenario (WLTC3b with a 6 kg tank).
- Like any other commercial vehicle, LCVs are subjected to intensive usage, making vehicle range a critical design parameter to fulfill the vehicle application requirements. Unsurprisingly, the range of the van directly correlates with the dimensions of both the FCS and the electric battery. However, having insight into the range provided by each specific architecture facilitates the selection of acceptable autonomies tailored to the desired vehicle mission. Furthermore, the findings reveal that enlarging both the battery and FCS significantly impacts vehicle autonomy, with the range increasing potentially reaching up to 116% for the 6 kg H_2 tank in WLTC3b conditions. This change in range is also influenced by the driving conditions and H_2 available in the vehicle, as this value changes to a 112% for the smaller tank and to 96% (6 kg tank) and 86% (4 kg tank) for WLTC2 conditions.
- The durability of the FCS stands as a crucial parameter in the design process of a FCV. The obtained results suggest that the durability of the FCS depends on both the propulsion system architecture and the operational conditions of the vehicle. Optimal designs for LCVs typically feature an FCS ranging between 45 and 60 kW, coupled with an electric battery from 20 to 33 kWh. Moreover, the results demonstrate a variability of up to 36% in durability when changing the powertrain design, which can be considered a first order effect. Besides, the change in the H_2 tank produces a variation up to a 3% in the results, which is a second order effect. Additionally, they indicate that load-change degradation mechanisms are the primary cause of degradation for such vehicles.
- The selection of powertrain architecture is intricately linked with the specific typical mission profile of the vehicle. Given that LCVs operate across diverse conditions, their propulsion systems must perform suitably across these scenarios. This paper demonstrates that a 60 kW FCS, together with a 33 kWh electric battery propulsion system incorporating a 6 kg H_2 tank, offers a viable solution for an LCV.

In conclusion, this study provides valuable insights into the performance and durability of the analyzed LCV designs. The data obtained offers a comprehensive understanding of how various component sizes within the powertrain impact the specific performance of an LCV. Overall, these findings highlight the importance of selecting a suitable powertrain architecture tailored to the unique mission profile of the vehicle. The proposed combination of a 60 kW FCS and 33 kWh electric battery system emerges as a promising solution for LCVs.

6. Future research prospects

This research introduces a significant degree of novelty and holds substantial value within the current industrial framework. Nevertheless, there remain areas for enhancement and the development of further studies that could use the obtained data as a starting point.

As detailed in Section 4, the dataset derived from the conducted simulation campaign provides valuable information for LCV manufacturers. These companies could use this data to perform a detailed analysis of the production costs associated with the different designs. However, a fair comparison of costs for consumers should incorporate the Total Cost of Ownership (TCO). Future research could, therefore, focus on developing a comprehensive and precise TCO analysis.

In the context of ongoing decarbonization efforts, the emissions generated by any technology are highly important. Consequently, it is crucial to analyze the emissions produced throughout the entire life cycle of the vehicle. This complex process requires a dedicated study, and future research should aim to develop a thorough LCA to calculate greenhouse gas (GHG) emissions across the lifespan of the vehicle.

Moreover, given that hydrogen (H_2) remains a relatively innovative energy vector, its various potential production pathways, projections for future scenarios, and comparisons with existing energy sources should be examined as part of the previously explained future LCA and TCO analyses.

The mentioned matters represent important challenges and will be considered in future studies. Despite their complexity, solving them would take FCS deployment in the transportation sector a step closer to becoming a reality.

CRediT authorship contribution statement

R. Novella: Supervision, Project administration, Funding acquisition, Conceptualization. **M. Lopez-Juarez:** Writing – original draft, Software, Resources, Methodology, Investigation, Data curation, Conceptualization. **D. González-Domínguez:** Software, Resources, Methodology, Conceptualization. **I. Nidaguila:** Writing – original draft, Validation, Methodology, Investigation, Conceptualization.

Declaration of competing interest

The authors declare that they have no known competing financial interests or personal relationships that could have appeared to influence the work reported in this paper.

Acknowledgments

This research has been partially funded by Universitat Politècnica de València through the support program for research and development (PAID-01-22) and by the Generalitat Valenciana (Conselleria d'Innovació, Universitats, Ciència i Societat Digital) as a part of the DEFIANCE research project (CIPROM/2021/039) through the PROMETEO funding program. The activities of this work are also part of TED2021-131463B-I00 (DIVERGENT) funded by MCIN/AEI/10.13039/501100011033 and the European Union "NextGenerationEU" /PRTR .

Data availability

Data will be made available on request.

References

[1] European Comission. A green deal industrial plan for the net-zero age. Tech. rep., Brussels; 2023.
[2] United Nations. Sustainable Transport Conference: Fact sheet climate chang. Tech. rep., 2021.
[3] International Energy Agency (IEA). Technology roadmap hydrogen and fuel cells. Tech. rep., Paris; 2015.
[4] Molina S, Gomez-Soriano J, Lopez-Juarez M, Olcina-Girona M. Evaluation of the environmental impact of HCNG light-duty vehicles in the 2020–2050 transition towards the hydrogen economy. Energy Convers Manage 2024;301:117968. http://dx.doi.org/10.1016/j.enconman.2023.117968.
[5] KoteswaraRao KV, Srinivasulu GN, Rahul JR, Velisala V. Optimal component sizing and performance of fuel cell – battery powered vehicle over world harmonized and new european driving cycles. Energy Convers Manage 2024;300:117992. http://dx.doi.org/10.1016/j.enconman.2023.117992.
[6] Study on hydrogen substitution in a compressed natural gas spark-ignition passenger car engine. Energy Convers Manage 2023;291:117259. http://dx.doi.org/10.1016/j.enconman.2023.117259.

[7] Pardhi S, Chakraborty S, Tran D-D, El Baghdadi M, Wilkins S, Hegazy O. A review of fuel cell powertrains for long-haul heavy-duty vehicles: Technology, hydrogen, energy and thermal management solutions. Energies 2022;15(24). http://dx.doi.org/10.3390/en15249557.

[8] Desantes JM, Novella R, Lopez-Juarez M, Nidaguila I. Experimental assessment of a heavy-duty fuel cell system in relevant operating conditions. Appl Energy 2024;376:124293. http://dx.doi.org/10.1016/j.apenergy.2024.124293.

[9] Yan J, Wang G, Chen S, Zhang H, Qian J, Mao Y. Harnessing freight platforms to promote the penetration of long-haul heavy-duty hydrogen fuel-cell trucks. Energy 2022;254:124225. http://dx.doi.org/10.1016/j.energy.2022.124225.

[10] Xu A, Yang Q, Yang L, Fan R, Liu C, Xie N, Yang S, Deng C. Life cycle assessment and carbon footprint evaluation of a PEMFC system integrated with different hydrogen production routes. Energy Convers Manage 2024;312:118586. http://dx.doi.org/10.1016/j.enconman.2024.118586.

[11] Ren L, Zhou S, Peng T, Ou X. Greenhouse gas life cycle analysis of China's fuel cell medium- and heavy-duty trucks under segmented usage scenarios and vehicle types. Energy 2022;249:123628. http://dx.doi.org/10.1016/j.energy.2022.123628.

[12] Ma R, Chai X, Geng R, Xu L, Xie R, Zhou Y, Wang Y, Li Q, Jiao K, Gao F. Recent progress and challenges of multi-stack fuel cell systems: Fault detection and reconfiguration, energy management strategies, and applications. Energy Convers Manage 2023;285:117015. http://dx.doi.org/10.1016/j.enconman.2023.117015.

[13] Chen J, He H, Wang Y-X, Quan S, Zhang Z, Wei Z, Han R. Research on energy management strategy for fuel cell hybrid electric vehicles based on improved dynamic programming and air supply optimization. Energy 2024;300:131567. http://dx.doi.org/10.1016/j.energy.2024.131567.

[14] Yang D, Wang L, Yu K, Liang J. A reinforcement learning-based energy management strategy for fuel cell hybrid vehicle considering real-time velocity prediction. Energy Convers Manage 2022;274:116453. http://dx.doi.org/10.1016/j.enconman.2022.116453.

[15] Li M, Wang Y, Yu P, Sun Z, Chen Z. Online adaptive energy management strategy for fuel cell hybrid vehicles based on improved cluster and regression learner. Energy Convers Manage 2023;292:117388. http://dx.doi.org/10.1016/j.enconman.2023.117388.

[16] Agyekum EB, Odoi-Yorke F, Abbey AA, Ayetor GK. A review of the trends, evolution, and future research prospects of hydrogen fuel cells – a focus on vehicles. Int J Hydrog Energy 2024;72:918–39. http://dx.doi.org/10.1016/j.ijhydene.2024.05.480.

[17] Zhan S, Liu C, Yin Y, Yu C, Zhao C. Eco-driving strategy for fuel cell vehicles in car-following scenarios considering stack heat and durability based on SAC. Energy Convers Manage 2024;315:118744. http://dx.doi.org/10.1016/j.enconman.2024.118744.

[18] Lee S, Kim MS. Stack cooling system coupled with secondary heat pump in fuel cell electric vehicles. Energy Convers Manage 2023;284:116961. http://dx.doi.org/10.1016/j.enconman.2023.116961.

[19] Silvestri L, Micco SD, Forcina A, Minutillo M, Perna A. Power-to-hydrogen pathway in the transport sector: How to assure the economic sustainability of solar powered refueling stations. Energy Convers Manage 2022;252:115067. http://dx.doi.org/10.1016/j.enconman.2021.115067.

[20] Chen X, Pang Z, Zhang M, Jiang S, Feng J, Shen B. Techno-economic study of a 100-MW-class multi-energy vehicle charging/refueling station: Using 100 superconductor technologies. Energy Convers Manage 2023;276:116463. http://dx.doi.org/10.1016/j.enconman.2022.116463.

[21] Molina S, Novella R, Pla B, Lopez-Juarez M. Optimization and sizing of a fuel cell range extender vehicle for passenger car applications in driving cycle conditions. Appl Energy 2021;285:116469. http://dx.doi.org/10.1016/j.apenergy.2021.116469.

[22] Skarlis S, Molos T, Ayfantopoulou G, Nikiforiadis A, Bakouros L. Light commercial electric vehicles with hydrogen fuel-cell range extender: Refueling strategy evaluation. Res Transp Bus Manag 2023;50:101040. http://dx.doi.org/10.1016/j.rtbm.2023.101040.

[23] Apostolou D. Refuelling scenarios of a light urban fuel cell vehicle with metal hydride hydrogen storage. Comparison with compressed hydrogen storage counterpart. Int J Hydrog Energy 2021;46(79):39509–22. http://dx.doi.org/10.1016/j.ijhydene.2021.09.157.

[24] Renault Press. Renault runs on hydrogen with master z.e. hydrogen and kangoo z.e. hydrogen. 2019.

[25] Yong C, Kreß J-P. Press kit: Opel vivaro-e HYDROGEN. 2022.

[26] Zachariah B. Hydrogen-fuelled Toyota HiAce twin-turbo V6 unveiled ahead of Australian pilot program. Drive 2023.

[27] Reeve N. Nissan unveils world's first solid-oxide fuel cell vehicle. Nissan Glob Newsroom 2016.

[28] Barbir F. PEM fuel cells theory and practice. Elsevier; 2013.

[29] Hydrogen and Fuel Cell Technologies Office. Types of fuel cells. Tech. rep., Office of Energy Efficiency and Renewable Energy; 2016.

[30] Kahraman H, Akın Y. Recent studies on proton exchange membrane fuel cell components, review of the literature. Energy Convers Manage 2024;304:118244. http://dx.doi.org/10.1016/j.enconman.2024.118244.

[31] Novella R, la Morena JD, Lopez-Juarez M, Nidaguila I. Effect of differential control and sizing on multi-FCS architectures for heavy-duty fuel cell vehicles. Energy Convers Manage 2023;293:117498. http://dx.doi.org/10.1016/j.enconman.2023.117498.

[32] Burke AF, Zhao J, Fulton LM. Projections of the costs of light-duty battery-electric and fuel cell vehicles (2020–2040) and related economic issues. Res Transp Econ 2024;105:101440. http://dx.doi.org/10.1016/j.retrec.2024.101440.

[33] Watabe A, Leaver J. Comparative economic and environmental benefits of ownership of both new and used light duty hydrogen fuel cell vehicles in Japan. Int J Hydrog Energy 2021;46(52):26582–93. http://dx.doi.org/10.1016/j.ijhydene.2021.05.141.

[34] Grady C, McWhorter S, Sulic M, Sprik SJ, Thornton MJ, Brooks KP, Tamburello DA. Design tool for estimating adsorbent hydrogen storage system characteristics for light-duty fuel cell vehicles. Int J Hydrog Energy 2022;47(69):29847–57. http://dx.doi.org/10.1016/j.ijhydene.2022.06.281.

[35] Tahir M, Hu S, Khan T, Zhu H. Sustainable hybrid station design framework for electric vehicle charging and hydrogen vehicle refueling based on multiple attributes. Energy Convers Manage 2024;300:117922. http://dx.doi.org/10.1016/j.enconman.2023.117922.

[36] Sagaria S, Neto RC, Baptista P. Assessing the performance of vehicles powered by battery, fuel cell and ultra-capacitor: Application to light-duty vehicles and buses. Energy Convers Manage 2021;229:113767. http://dx.doi.org/10.1016/j.enconman.2020.113767.

[37] Zhou Y, Li H, Ravey A, Péra M-C. An integrated predictive energy management for light-duty range-extended plug-in fuel cell electric vehicle. J Power Sources 2020;451:227780. http://dx.doi.org/10.1016/j.jpowsour.2020.227780.

[38] Hu D, Hou W, Cheng Z, Feng C, Lu D, Yi F, Yang Q, Li J, Wang J. A temperature fluctuation suppression control method of fuel cell vehicles to reduce hydrogen consumption. Energy 2024;305:132378. http://dx.doi.org/10.1016/j.energy.2024.132378.

[39] Pan R, Yang D, Wang Y, Chen Z. Health degradation assessment of proton exchange membrane fuel cell based on an analytical equivalent circuit model. Energy 2020;207:118185. http://dx.doi.org/10.1016/j.energy.2020.118185.

[40] Huang W, Niu T, Zhang C, Fu Z, Zhang Y, Zhou W, Pan Z, Zhang K. Experimental study of the performance degradation of proton exchange membrane fuel cell based on a multi-module stack under selected load profiles by clustering algorithm. Energy 2023;270:126937. http://dx.doi.org/10.1016/j.energy.2023.126937.

[41] Desantes J, Novella R, Pla B, Lopez-Juarez M. A modeling framework for predicting the effect of the operating conditions and component sizing on fuel cell degradation and performance for automotive applications. Appl Energy 2022;317:119137. http://dx.doi.org/10.1016/j.apenergy.2022.119137.

[42] Lopez-Juarez M, Rockstroh T, Novella R, Vijayagopal R. A methodology to develop multi-physics dynamic fuel cell system models validated with vehicle realistic drive cycle data. Appl Energy 2024;358:122568. http://dx.doi.org/10.1016/j.apenergy.2023.122568.

[43] Blanc H. HYVIA: leading green H_2 mobility. 2022.

[44] Onori S, Serrao L, Rizzoni G. Hybrid electric vehicles: Energy management strategies. Springer London; 2016, http://dx.doi.org/10.1007/978-1-4471-6781-5.

[45] Lujan JM, Guardiola C, Pla B, Reig A. Cost of ownership-efficient hybrid electric vehicle powertrain sizing for multi-scenario driving cycles. Proc Inst Mech Eng D 2016;358:122568. http://dx.doi.org/10.1177/0954407015586333.

[46] Pei P, Chang Q, Tang T. A quick evaluating method for automotive fuel cell lifetime. Int J Hydrog Energy 2008;33:3829–36. http://dx.doi.org/10.1016/j.ijhydene.2008.04.048.

[47] Popovich N. 2015 Annual Progress Report: DOE Hydrogen and Fuel Cells Program.

[48] Knights S. 6 - operation and durability of low temperature fuel cells. In: Hartnig C, Roth C, editors. Polymer electrolyte membrane and direct methanol fuel cell technology. Woodhead publishing series in energy, vol. 1, Woodhead Publishing; 2012, p. 137–77. http://dx.doi.org/10.1533/9780857095473.2.137.

[49] Bi W, Fuller T. Temperature effects on PEM fuel cells pt/c catalyst degradation. ECS Trans 2007;11(1):1235. http://dx.doi.org/10.1149/1.2781037.

[50] Dutta M, Jia N, Lu S, Colbow V, Wessel S. Effects of upper potential dwell time, transients and relative humidity on PEM fuel cell cathode catalyst degradation. In: ECS meeting abstracts. vol. MA2010-01, 2010, http://dx.doi.org/10.1149/MA2010-01/9/543.

[51] Desantes J, Novella R, Pla B, Lopez-Juarez M. Effect of dynamic and operational restrictions in the energy management strategy on fuel cell range extender electric vehicle performance and durability in driving conditions. Energy Convers Manage 2022;266:115821. http://dx.doi.org/10.1016/j.enconman.2022.115821.

[52] Department for Transport . Final van statistics 2019-20. 2021.

[53] Multi-drop driving: What are the risks? 2024, ©2024 DriverMetrics® limited, a wholly owned subsidiary of a2om® International Limited.

[54] Yewdale. A day in the life of an elite delivery driver. 2024.

[55] Basma H, Rodríguez F, Hildermeier J, Jahn A. Electrifying LAST-mile DELIVERY a total cost of ownership comparison of battery-electric and diesel trucks in Europe. 2022.